# Spatiotemporal patterns and localized structures in nonlinear optics

M. Tlidi and Paul Mandel
*Optique Nonlinéaire Théorique, Université Libre de Bruxelles, Campus Plaine, Code Postal 231, B-1050 Bruxelles, Belgium*

M. Haelterman
*Laboratoire d'Optique et d'Acoustique, Université Libre de Bruxelles, Code Postal 1945, 50 Avenue F.D. Roosevelt, B-1050 Bruxelles, Belgium*

(Received 30 June 1997)

We show that in a degenerate optical parametric oscillator with saturable losses for the frequency down-converted field, the steady state can be destabilized via either a Hopf or a Turing instability. The relative order between the two bifurcations is controlled by the linear loss of the saturable absorber. If the Turing bifurcation is subcritical and the Hopf bifurcation occurs in the hysteresis domain involving the homogeneous and inhomogeneous states, steady localized structures are generated below the Hopf bifurcation and time-periodic localized structures are generated above the Hopf bifurcation. [S1063-651X(97)01912-0]

PACS number(s): 05.40.+j, 42.65.Sf, 42.60.Mi

## I. INTRODUCTION

Localized structures (LS's) are solitonlike (i.e., homoclinic) solutions of partial differential equations that connect coexisting stable homogeneous and inhomogeneous steady states. This situation is realized, for instance, by a subcritical Turing instability. In optics, an early report on localized structures was given in [1], which described numerical simulations of pulse propagation in bistable systems. Later on it was shown that the existence of LS's does not require a bistable homogeneous steady state. They were analyzed more systematically in [2] in relation with a generalized Swift-Hohenberg equation. Analytical results on homoclinic solutions of this equation are found in [3]. More recently, LS's have been obtained in an absorptive nonlinear optical system [4]. The purpose of this paper is to analyze the interaction of Turing and Hopf instabilities in a nonlinear optical system and to study the implications of this interaction in the dynamics of the LS's. Such an interaction has been investigated in nonlinear chemistry and hydrodynamics where it stems from reaction-diffusion equations [5]. The results of these analyses have been compared with experiments [6]. The main difference brought in by considering optical systems is that the diffusion is often replaced by diffraction. When the system is nonlinear this leads to reaction-diffraction equations, which modifies completely the stability problem. For instance, negative diffusion leads to unstable solutions, while the diffraction coefficient may be positive or negative, corresponding to beam focusing or defocusing. Furthermore, the diffraction coefficient is essentially the inverse of the photon wave number that is constrained by the momentum conservation law. Hence it cannot be varied freely. In optics, time-dependent transverse periodic patterns have been studied numerically in a bistable system where the Hopf bifurcation is on the lower branch and the Turing bifurcation is on the upper branch [7]. In this model, the Lugiato-Lefever equation (the LL model includes diffraction [8]) for the field is coupled to a diffusion equation modeling the nonlocal response of the nonlinear medium. For the degenerate optical parametric oscillator, it was shown that the Hopf bifurcation always appears after the Turing instability on the branch of steady-state solutions and that the distance between the two instabilities cannot be made arbitrarily small [9]. A similar result holds for intracavity second-harmonic generation. In both cases, the impossibility to control the relative position of the two bifurcations is due to the fact that the ratio of the diffraction coefficients is either 2 or 1/2 and cannot be varied. This results from the phase-matching condition [10]. A completely different mechanism for the generation of time-periodic transverse patterns is a Hopf bifurcation emerging on the Turing branch as a secondary bifurcation. In this case, the Hopf instability arises from the nonlinear interaction between transverse modes. This mechanism was described in [11] for two counterpropagating coherent beams in a Kerr medium and in [12] for the LL model.

This paper is organized as follows. After briefly introducing the model of the degenerate optical parametric oscillator (Sec. II), we present a linear stability analysis of its nontrivial homogenous steady-state solutions (Sec. III). The analytical and numerical analysis of the interaction between the Turing and Hopf instabilities is described in Sec. IV on the basis of a normal form analysis. Stationary and time-periodic localized structures are studied in Sec. V in relation with the various dynamical behaviors identified in the bifurcation diagrams derived in Sec. IV. We conclude in Sec. VI.

## II. DESCRIPTION OF THE MODEL

In this paper we consider a degenerate optical parametric oscillator (DOPO) driven by an external field at frequency $2\omega$. This field is converted by a quadratic nonlinear medium into a field at frequency $\omega$. In addition, we assume the presence of a saturable absorber (SA) that acts selectively on the field at frequency $\omega$. Saturable absorption is modeled by a collection of two-level atoms that leads to an intensity-dependent effective absorption coefficient. This model for the DOPOSA was introduced in [14]. Assuming fast atomic relaxation, the evolution equations in reduced variables are

 

$$\frac{\partial E_1}{\partial t} = -E_1 + E_1^* E_2 - \frac{R E_1}{1+S|E_1|^2} + 2i\mathcal{L}_\perp E_1, \tag{1}$$

$$\frac{\partial E_2}{\partial t} = -\gamma(E_2 + E_1^2 - E_I) + i\mathcal{L}_\perp E_2. \tag{2}$$

In these equations, $E_j$ is the field at frequency $j\omega$, $E_I$ is the driving field which is chosen real by convention, and $\gamma$ is the ratio of the photon lifetimes at frequencies $\omega$ and $2\omega$. The saturable absorber is characterized by its saturation intensity $(1/S)$ and its linear loss coefficient $R$. $\mathcal{L}_\perp$ is the transverse Laplacian. Time has been scaled such that the decay rate of the field $E_1$ is unity. Note that we assume, for the sake of simplicity, that both fields are resonant with the optical cavity (i.e., zero cavity detunings).

## III. LINEAR STABILITY ANALYSIS

Equations (1) and (2) have two types of homogeneous steady-state solutions, with $E_1$ equal to or different from zero

$$\overline{E_1} = 0, \quad \overline{E_2} = E_I, \tag{3}$$

$$E_I = 1 + |\overline{E_1}|^2 + \frac{R}{1+S|\overline{E_1}|^2}, \quad \overline{E_2} = E_I - \overline{E_1^2}, \tag{4}$$

where the overbar refers to steady states. For $RS<1$ $(RS>1)$ the steady-state intensity $|\overline{E_1}|^2$, as a function of $E_I$, is monostable (bistable). The solution (3) is stable when $E_I<E_{th}=1+R$. The nonlasing (3) and the lasing (4) solutions coincide at $E_I=E_{th}$. We perform a linear stability analysis of the steady state. With transverse periodic boundaries, the linear deviation from the steady lasing state is proportional to $\exp(\lambda t + i\mathbf{k}\cdot\mathbf{r})$, where $\mathbf{r}$ stands for the transverse coordinates and the transverse wave vector $\mathbf{k}$ verifies the relation $(\mathcal{L}_\perp + k^2)\exp(i\mathbf{k}\cdot r) = 0$. This formulation leads to a characteristic polynomial that is quartic in $\lambda$ and whose coefficients are functions of $K \equiv k^4$. For the variables $u_{1,2} = E_{1,2} - \overline{E}_{1,2}$ and $u_{1,2}^* = E_{1,2}^* - \overline{E}_{1,2}^*$, the quartic polynomial is

$$P(4,\lambda) = \sum_{l=0}^{4} f_n \lambda^n, \tag{5}$$

where

$$f_4 = 1, \tag{6}$$

$$f_3 = 2(\gamma - \beta_-), \tag{7}$$

$$f_2 = 4\gamma|\overline{E_1}|^2 - 4\gamma\beta_- + 5K + \beta_-^2 - \beta_+^2 + \gamma^2, \tag{8}$$

$$f_1 = 2\gamma(\beta_-^2 - \beta_+^2) + 4\gamma|\overline{E_1}|^2(\gamma - \beta_-) - 2\beta_-(\gamma^2 + K) + 8\gamma K, \tag{9}$$

$$f_0 = (\beta_-^2 - \beta_+^2 + 4K)(\gamma^2 + K) - 4\gamma|\overline{E_1}|^2 \times (\gamma\beta_- + 2K - \gamma|\overline{E_1}|^2), \tag{10}$$

with

$$\beta_\pm = \pm 1 \pm \alpha R(1 \pm \alpha S|\overline{E_1}|^2), \quad \alpha = \frac{1}{1+S|\overline{E_1}|^2}.$$

Turing instabilities correspond to the occurrence of a zero real root (i.e., $f_0 = 0$) of the characteristic polynomial with $K \neq 0$. The equation $f_0 = 0$ determines the intrinsic wave number $k_T$ and the critical-field amplitude $E_{1T}$ at which the Turing bifurcation takes place. This equation is implicit since the relation between the field of mode 1 and the input field is given by Eqs. (4).

Hopf bifurcations occur if a pair of complex-conjugate roots has a vanishing real part and a nonzero imaginary part. Our calculations show that there can be zero, one, or two Hopf bifurcations. The critical intensities of mode 1 at the Hopf bifurcations are

$$|\overline{E_{1H\pm}}|^2 = \frac{R - \gamma \pm \sqrt{R(R-2\gamma)}}{\gamma S}.$$

The number of Hopf bifurcations is determined by the reality condition of $|\overline{E_{1H\pm}}|^2$. The frequency of the periodic solutions that emerges at the Hopf bifurcation is $\Omega_H^2 = \gamma(2|\overline{E_{1H\pm}}|^2 - \gamma)$. An exhaustive classification of the bifurcation diagram for the homogeneous steady-state solutions is given in [14].

We fix $\gamma = 1$, $S = 0.1$, and let $R$ and $E_I$ be the control parameters. For these parameters, there are two Hopf bifurcations. We concentrate on the Hopf bifurcation that has the lower-intensity threshold. We find that there is a critical linear loss $R_c \approx 5.47$ such that for $R$ larger (smaller) than $R_c$ the Hopf bifurcation occurs after (before) the Turing instability. For $R = R_c$, the system undergoes both instabilities for the same value of the input intensity. In Fig. 1 we display the bifurcation diagrams of the steady-state solutions in the parameter plane $(I_1 \equiv |\overline{E_1}|^2, k^4)$. We show in this figure the stable and unstable domains associated with inhomogeneous perturbations.

We stress that this analysis is performed only for the homogeneous lasing solution (4). A similar stability analysis shows that the homogeneous nonlasing solution (3) is always stable against small transverses perturbations. Note also that, in the absence of saturable absorber $(S=0)$, the Turing instability can occur on the trivial solution branch, i.e., $E_I < E_{th}$ [9].

## IV. INTERACTION BETWEEN TURING AND HOPF INSTABILITIES

### A. Amplitude equations

We have shown in Sec. III that the DOPOSA model exhibits Turing and Hopf bifurcations leading to steady inhomogeneous transverse and/or homogeneous temporal-periodic patterns. The main point now is to study the stability of the emerging branches, in particular to show analytically that the system can exhibit a bistability between the Hopf and Turing branches. To this end, we develop a standard nonlinear analysis and derive amplitude equations. To capture analytically the nature of the interaction between the

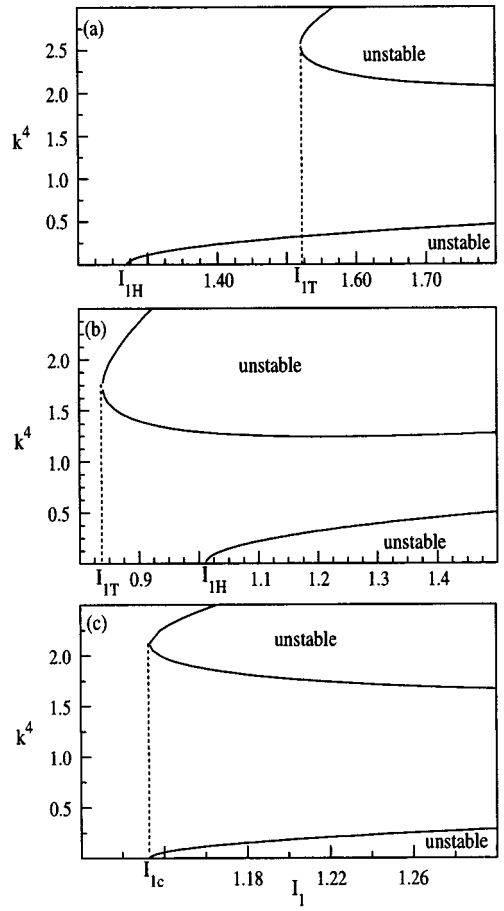


FIG. 1. Linear stability curves associated with the Hopf and the Turing solutions. We plot the fourth power of the transverse wave number versus the homogeneous intensity $I_1=|\overline{E_1}|^2$. The parameters are $\gamma=1.0$ and $S=0.1$. By changing the value of the pump parameter $R$, we can distinguish beteween three cases: (a) $R=5.0$, (b) $R=6.0$, and (c) $R=5.47$.

Hopf and Turing branches, we work in the vicinity of the codimension-2 point $E_I=E_{IH}=E_{IT}$, where the two bifurcations coincide. At this point, one of the real roots of the characteristic equation (5) vanishes (with a finite intrinsic wave number $k=k_c\neq 0$) and two others roots are purely imaginary $\lambda=\pm i\Omega_H$. Near this critical point, the dynamics of the system can be described by a linear superposition of the Hopf and the Turing solutions $H(t)\mathbf{1}_H\exp(i\Omega_H t)+M(t)\mathbf{1_M}\exp(ik_c x)+$c.c., where $\mathbf{1}_H$ and $\mathbf{1}_M$ are the eigenvectors of the linearized operator derived from Eqs. (1) and (2) and $H(t)$ and $M(t)$ are, respectively, the amplitude of the Hopf and the Turing modes. By performing an expansion in terms of a small parameter that measures the distance from the critical point, the evolution equation of the amplitudes $H(t)$ and $M(t)$ can be obtained from the solvability condition. Such an analysis has been performed in the case of reaction-diffusion systems where the Hopf and the Turing bifurcations are both supercritical [5]. If the Turing bifurcation is supercritical, third-order terms are sufficient to provide the evolution equations of the amplitude functions. If the Turing bifurcation is subcritical, fifth-order terms are necessary. In this case, the evolution of the amplitude associated with the Turing and the Hopf solutions [13] is given by

$$\frac{\partial M}{\partial t}=\mathcal{M}M+l_2|H|^2M+l_3|M|^2|H|^2M+l_4|H|^4M, \tag{11}$$

$$\frac{\partial H}{\partial t}=\mathcal{H}H+(k_2+ik_2')|M|^2H+(k_3+ik_3')|H|^2|M|^2H+(k_4+ik_4')|M|^4H, \tag{12}$$

where $\mathcal{M}=\beta_m+l_1|M|^2-|M|^4$ and $\mathcal{H}=\beta_h+i\beta_h'-(1+ik_0)|H|^2+(k_1+ik_1')|H|^4$. The coefficients $\beta_m=E_I-E_{IT}$ and $\beta_h=E_I-E_{IH}$ measure, respectively, the distance from the Turing and the Hopf bifurcations. In the vicinity of the codimension-2 point, the coefficient $l_1$ is always positive, which means that the Turing branch emerges subcritically from the lasing homogeneous state. Hence, for $\beta_m>0$, the stable solution is on the upper (i.e., large amplitude) branch of solutions. On the other hand, the Hopf oscillatory branch is supercritical: Oscillation amplitudes vanish as $\beta_h\to 0$. The amplitude of the Hopf solution is therefore expected to be much smaller than the amplitude of the Turing structure. In the following discussion, we therefore neglect the terms proportional to $|H|^4$. Furthermore, we impose, for mathematical simplicity, $k_3=k_4=0$. As will be seen in Sec. IV B, these approximations are in good agreement with the numerical simulations. In addition, we eliminate adiabatically the phases $\Phi_m$ and $\Phi_h$, which are introduced through the polar decompositions $M=m\exp(i\Phi_m)$ and $H=h\exp(i\Phi_h)$. Under these approximations, the dynamics of the DOPOSA near the codimension-2 point admits four types of solutions: (i) the uniform solution $m_0=0$ and $h_0=0$, (ii) the pure Turing solution $m_{1s,2s}^2=(l_1\pm\sqrt{l_1^2+4\beta_m})/2$, (iii) the pure Hopf solution $h_{0s}=\pm\sqrt{\beta_h}$, and (iv) the Hopf-Turing mixed-mode solution $M_{1s,2s}^2=[-k\pm\sqrt{k^2-4(k_2l_3-1)(\beta_m+l_2\beta_h)}]/2(k_2l_3-1)$ and $H_{1s,2s}^2=\beta_h+k_2M_{1s,2s}^2$, where $k=k_2l_2+l_3\beta_h+l_1$.

For now, we restrict our analysis to the domain of parameter space in which the Hopf bifurcation is the primary instability: $\beta_h-\beta_m=E_{IT}-E_{IH}>0$. Let us begin with the study of the linear stability of the solutions (i)–(iv). The trivial solution (i) becomes unstable when $\beta_h>0$. We perturb the pure Turing solution (ii) as $M=m_{1s,2s}+u$ and $H=v$, with $u,v\ll 1$. We substitute these relations into the simplified real form of the amplitude equations (11) and (12) and upon linearization we obtain

$$\frac{\partial u}{\partial t}=-2\xi_1 u,\quad \frac{\partial v}{\partial t}=\xi_2 v, \tag{13}$$

where $\xi_1=2\beta_m+l_1m_{1s,2s}^2$ and $\xi_2=2\beta_h+k_2m_{1s,2s}^2$. From Eq. (13) we deduce that the Turing solution (ii) is stable when the two conditions are met: $\xi_1>0$ and $\xi_2<0$. Similarly, the linear stability analysis of the solution (iii) shows that the pure Hopf solution (iii) remains stable for $\beta_h>0$ only if $\beta_m>k_2\beta_h$. Finally, the linear stability of Hopf-Turing solution (iv) shows that it is stable if the roots of the quadratic polynomial $\Lambda^2-(\mu+\nu)\Lambda+(\mu+\sigma)\nu=0$ are both negative, with

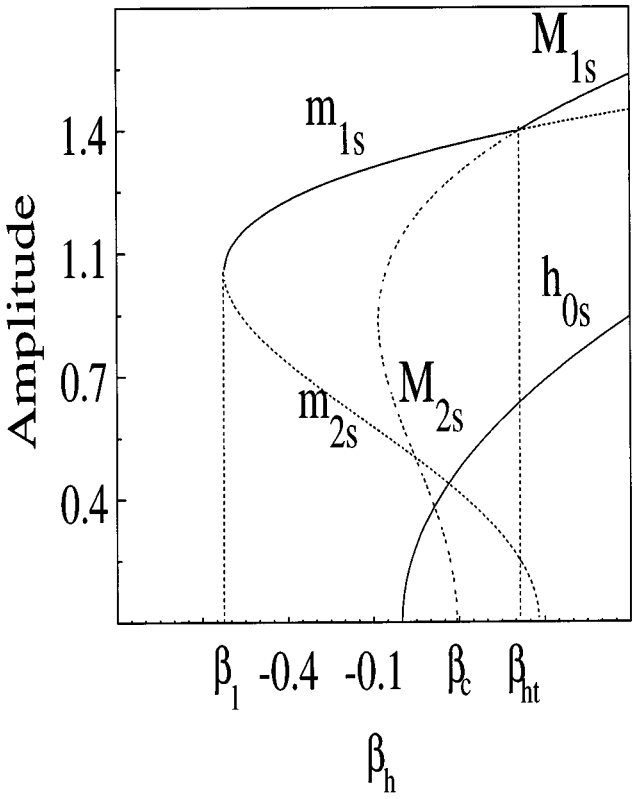


FIG. 2. Bifurcation diagram obtained from the normal form analysis. The full and the dotted lines correspond, respectively, to stable and unstable solutions. The parameters are $l_1=2.1$, $l_2=1.5$, $l_3=0.6$, and $k_2=-0.2$. $\beta_c=E_{IT}-E_{IH}$ is the distance between the two thresholds associated with the Turing and the Hopf bifurcation.

$$\mu=\beta_m+l_2\beta_h+[(3k_2l_3-5)M_{1s,2s}^2+3l_1+k_2l_2+3l_3\beta_h]M_{1s,2s}^2, \tag{14}$$

$$\nu=2k_2(l_3M_{1s,2s}^2+l_2), \quad \sigma=-2(\beta_h+k_2M_{1s,2s}^2). \tag{15}$$

The results of the above stability analysis are summarized in the bifurcation diagram displayed in Fig. 2, where we have plotted the amplitude of the solutions (i)–(iv) versus $\beta_h$. Both the pure Turing and Hopf-Turing branches appear subcritically, while the homogeneous Hopf branch emerges supercritically. For larger values of $\beta_h$, the steady inhomogeneous solution $m_{2s}$ emerges from the homogeneous solution at the Turing point and is unstable until it reaches a limit point $\beta_h=\beta_l$ from which the branch $m_{1s}$ emerges stably. As a consequence of this subcriticality, there is a domain $\beta_l<\beta_h<0$ of bistability between the Turing branch and the homogeneous steady-state branch. This solution becomes unstable for $\beta_h>0$ and a stable Hopf branch $h_{0s}$ is observed. On the other hand, the Turing branch persists up to the value $\beta_h=\beta_{ht}$. As can be seen in Fig. 2, there is a finite domain $0<\beta_h<\beta_{ht}$ in which there is bistability between the Hopf and the Turing branches.

Above the transition point $\beta_h=\beta_{ht}$ the Turing branch becomes unstable and the dynamics of the system give way to Hopf-Turing solutions. However, the pure Hopf oscillatory solution remains stable and coexists with the Hopf-Turing solutions.

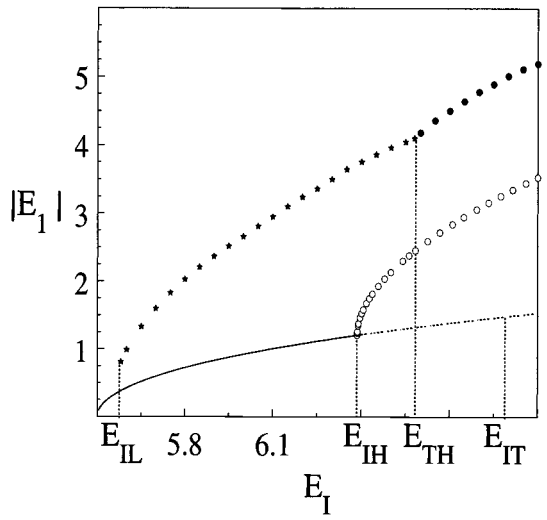


FIG. 3. Bifurcation diagram obtained numerically for the field $|E_1|$ at the frequency $\omega$ versus $E_I$. The parameters are $R=4.5$, $S=0.1$, and $\gamma=1$. The full and the dotted lines indicate, respectively, the stable and unstable homogeneous steady states. The stars indicate the difference between the maximum and minimum Turing amplitudes. The black (white) circles correspond to the difference between the maximun and minimum Hopf-Turing mixed-mode (Hopf) amplitudes.

### B. Numerical simulations

Our numerical simulations are concentrated on the parameter range corresponding to monostability of the steady-state homogeneous solutions $RS<1$ and to a leading Hopf bifurcation $E_{IH}<E_{IT}$. In this way, we can directly compare our results with those of the normal form analysis derived in the preceding subsection. To this end, we choose $R=4.5$, $S=0.1$, and $\gamma=1$. The corresponding bifurcation diagram is shown in Fig. 3. The Turing bifurcation at $E_{IT}$ is subcritical and generates a domain of bistability $E_{IL}<E_I<E_{IT}$. The upper branch corresponds to stable stripes (the numerical simulations are performed with one transverse dimension) that fill the transverse plane. Stars on the upper branch give the maximum of the stripe amplitude. At $E_I=E_{IH}$, a supercritical Hopf bifurcation takes place.

We have verified that the stripes displayed in Fig. 3 are stable. Stability means here that taking the stripe structure obtained for a given $E_{I1}$ as an initial condition, integration of Eqs. (1) and (2) for $E_I=E_{I1}\pm\varepsilon$ yields a new stripe pattern with the same wave number but a slightly modified amplitude. The time-periodic solutions that emerge from the Hopf bifurcation are obtained by taking as initial condition the unstable homogeneous state perturbed by a small-amplitude white noise. In the long-time limit, we obtain a homogeneous solution in which all points oscillate with the same phase and amplitude. The numerical results, displayed in Fig. 3, provide evidence for the fact that stable Turing structures and homogeneous Hopf solutions coexist in the domain $E_{IH}<E_I<E_{TH}$. Note that bistability between the pure Hopf and Turing solutions as a dominant dynamical behavior has been observed in two-component reaction-diffusion systems [5,6].

In the domain $E_I>E_{TH}$, Turing solutions become unstable and give way to Hopf-Turing solutions. These solu-

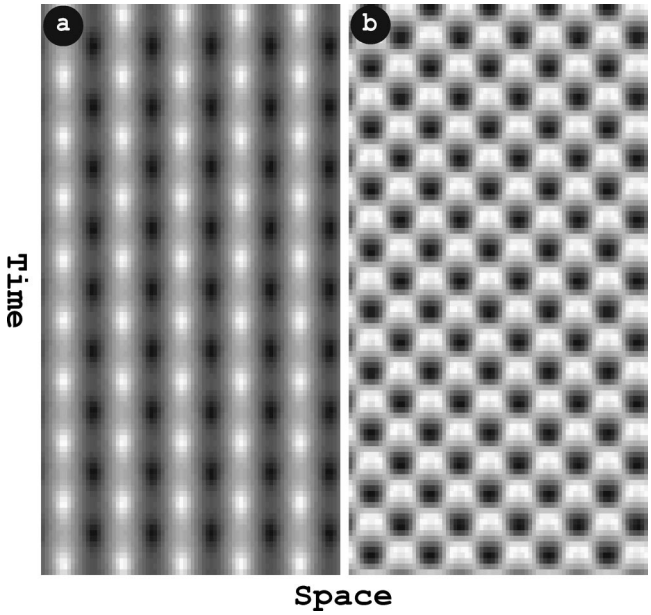


FIG. 4. Time-space map for the Hopf-Turing mixed-mode solutions. The parameters are $\gamma=1$, $R=4.5$, $S=0.1$, and $E_I=6.78$. (a) Real part of the electric field $E_1$. (b) Real part of the electric field $E_2$. Maxima are plain white and mesh number integration is 80.

tions naturally exhibit oscillations in both space and time. Such solutions are illustrated in Fig. 4. Note that for $E_I>E_{TH}$ there is also bistability between the mixed Hopf-Turing branch and the pure Hopf solutions.

As we shall see in the following section, the occurrence of bistability between the pure Hopf branch and either the pure Turing or Hopf-Turing mixed-mode branches leads to a large class of localized patterns. This problem is analyzed in the following section.

## V. STATIONARY AND TIME-PERIODIC LOCALIZED STRUCTURES

The numerical simulations reported in this section are obtained in one transverse dimension, using periodic boundary conditions. Let us consider the various domains of input field amplitude that appear in the bifurcation diagram of Fig. 3. As we shall see, different types of localized structures exist that are associated with each of these domains. We consider here only a numerical study of these solutions, an analytical approach to the problem being far beyond the scope of the present report. For $E_{IL}<E_I<E_{IH}$ corresponding steady stripes (pure Turing branch, see Sec. IV B) we have observed steady LS's. The LS's connect the branch of Turing patterns (in this case, the stripes) and the stable homogeneous solution. Two examples of steady LS's are displayed in Figs. 5(a) and 5(b). The difference between both cases is due only to the initial condition, all other parameters being the same. They have the same properties as those analyzed in [2,15]. In the domain $E_{IH}<E_I<E_{TH}$, the homogeneous time-periodic solution coexists with steady stripes. Time-periodic LS's associated with these coexisting solutions have been observed. A typical space-time configuration of the electric field is shown in Figs. 5(c) and 5(d). In this example the LS consists of two stationary peaks. Their amplitude and the distance between them are essentially those of the Turing structure. In

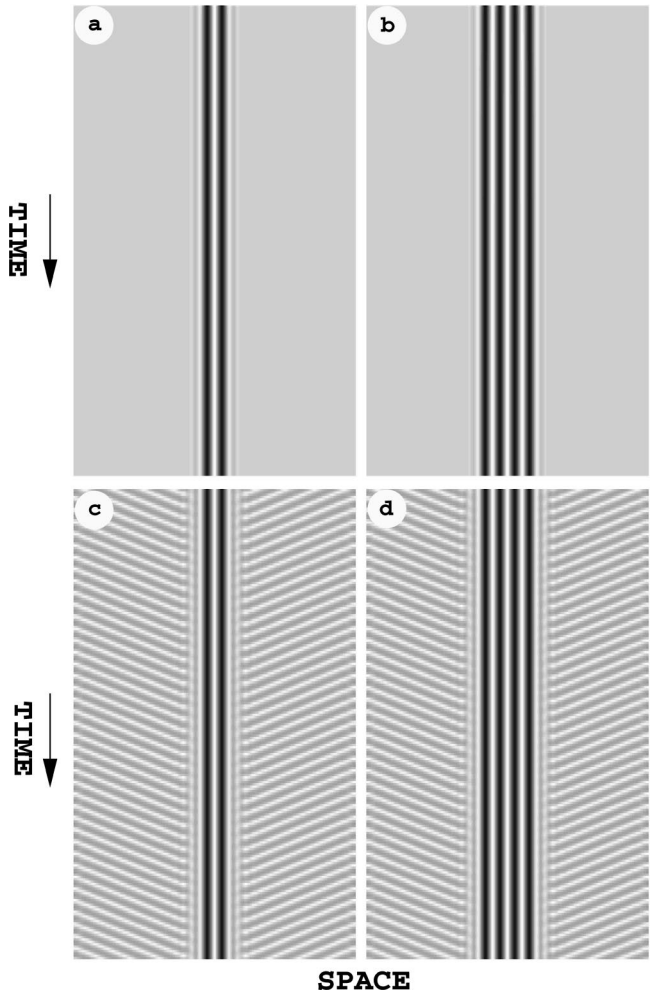


FIG. 5. Localized patterns. Same parameters as in Fig. 3. The real part of $E_1$ is plotted in the time and transverse space coordinate plane. The color code is the same for the four figures: Re($E_1$) varies from its minima (black) to its maxima (white). (a) and (b) Steady localized structures for $E_I=5.8$. (c) and (d) Self-pulsing localized structures for $E_I=6.5$. The mesh number for transverse integration is 300.

order to seed a LS, the initial homogeneous state has been perturbed by a local amplitude increase. Such perturbations evolve rapidly towards stable LS's. The number of peaks of the LS depends on the initial condition. Note that the unperturbed background should undergo the Hopf instability and oscillate homogeneously. However, it appears that this time-periodic structure (pure Hopf mode) is unstable against the growth of traveling waves (TW's). The simulations show that these TW's propagate with opposite directions on each side of the peaks. These TW's have the form $\exp[i(2\pi/\Lambda_{TW})(x\pm vt)]+$c.c. The wavelength $\Lambda_{\mathrm{TW}}$ selected by the nonlinear dynamics is not linked to the Turing wavelength and the amplitude of the TW's is smaller than that of the Turing structure. This feature is illustrated in Fig. 6, where the time-periodic LS of Fig. 5 is represented at three different times. Clearly the TW's originate from the wings of the LS. Therefore, they appear to be the result of a nonlinear interaction between the homogeneous Hopf modes and the LS. Let us notice that the temporal frequency of the TW's corresponds to the frequency of the pure Hopf solution ob-

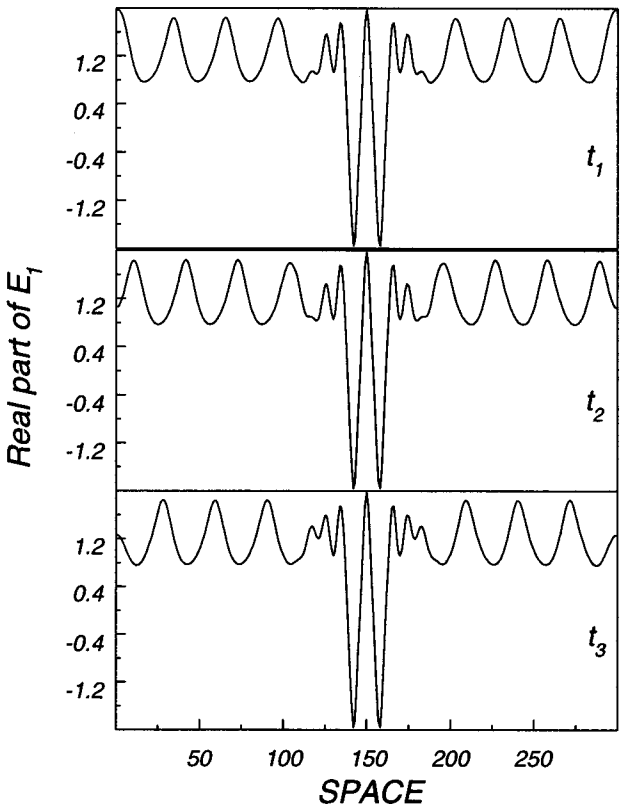


FIG. 6. Three sections taken from Fig. 5(c). The time sequence is $t_1<t_2<t_3$.

served in the absence of LS (i.e., $v=\Omega_H\Lambda_{\mathrm{TW}}/2\pi$).

As the input electric field is further increased, the Turing structures become unstable and give rise to the Hopf-Turing mixed mode at $E_I=E_{TH}$, as discussed in Secs. III and IV. In the domain $E_I>E_{TH}$, the Hopf homogeneous oscillatory solution coexists with the stable Turing-Hopf space- and time-periodic pattern. In this domain, another class of time-periodic LS's is observed. They are illustrated in Fig. 7. They consist of oscillating multiple peaks originating from the Hopf-Turing mixed mode, surrounded by traveling waves propagating in opposite directions. The number of oscillating peaks included in the LS depends only on the initial condition.

## VI. CONCLUSION

In conclusion, by using the normal form analysis for the description of the dynamics of a degenerate optical parametric oscillator with saturable absorber in the vicinity of the codimension-two point, we have studied the interaction between subcritical Turing and supercritical Hopf bifurcations. This analysis reveals the existence of a domain in which

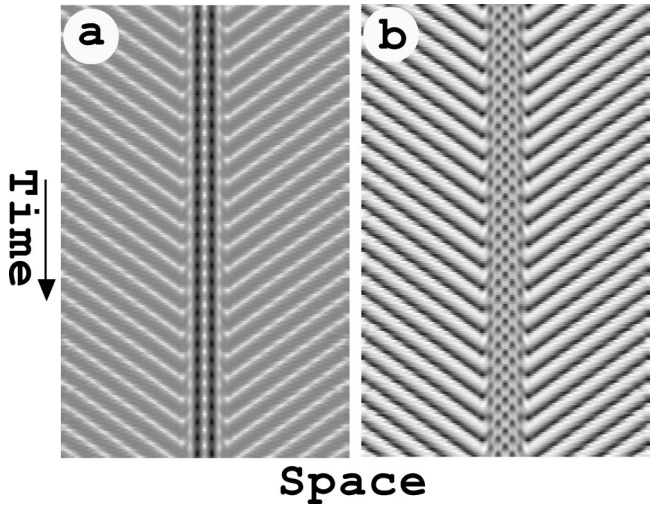


FIG. 7. Bands of the localized Hopf-Turing mixed-mode solution surrounded by diverging traveling waves. The parameters are $\gamma=1$, $R=4.5$, $S=0.1$, and $E_I=6.78$. (a) Real part of the electric field $E_1$. (b) Real part of the electric field $E_2$. Maxima are plain white and the mesh number integration is 300.

bistability between the Turing structures and the Hopf solutions occurs. Such behaviors have been described in reaction-diffusion processes where the two bifurcations are both supercritical [5,6]. As the input field amplitude is further increased, the Turing structures lose their stability and we observe the coexistence of Hopf-Turing spatio-temporal structures and the pure Hopf modes. These results obtained from the normal form analysis are supported by numerical simulations of the full dynamical model [Eqs. (1) and (2)]. We have shown that the coexistence of different types of solutions (stationary and/or time periodic) is associated with a large variety of localized structures. A numerical study of pattern formation in the DOPOSA, performed with the help of a detailed analysis of the bifurcation diagrams, allowed us to identify previously unrecognized time-periodic localized structures. Our predictions are applicable to other nonlinear systems and are important for the identification and the understanding of the various spatiotemporal behaviors observed in practical devices. The bifurcation analysis of the two-transverse-dimensional problem will be the subject of future work.

## ACKNOWLEDGMENTS

Fruitful discussions with P. Borckmans, G. Dewel, and R. Lefever are gratefully acknowledged. This research was supported in part by the Fonds National de la Recherche Scientifique (Belgium) and the Inter-University Attraction Pole Program of the Belgian government.

[1] N. N. Rosanov and G. V. Khodova, Opt. Spektrosk. **72**, 1394 (1992); a review of this group's activity is presented in N. N. Rosanov, Proc. SPIE **1840**, 130 (1992).

[2] M. Tlidi, P. Mandel, and R. Lefever, Phys. Rev. Lett. **73**, 640 (1994).

[3] L. Yu. Glebsky and L. M. Lerman, Int. J. Nonlinear Sci. **5**, 424 (1995).

[4] W. J. Firth and A. J. Scroggie, Phys. Rev. Lett. **76**, 1623 (1996); M. Brambilla, L. A. Lugiato, and M. Stefani, Europhys. Lett. **34**, 109 (1996).

[5] G. Nicolis, T. Erneux, and M. Hershkowitz-Kaufman, Adv. Chem. Phys. **38**, 263 (1978); H. Kidachi, Prog. Theor. Phys. **63**, 1152 (1980); A. B. Rovinsky and M. Menzinger, Phys. Rev. A **46**, 6315 (1992).

[6] P. Koldner, Phys. Rev. E **48**, 665 (1993); J. J. Perraud *et al.*, Phys. Rev. Lett. **71**, 1272 (1993); G. Heidemann *et al.*, Phys. Lett. A **177**, 225 (1993).

[7] J. Danckaert and G. Vitrant, Opt. Commun. **104**, 196 (1993).

[8] L. A. Lugiato and R. Lefever, Phys. Rev. Lett. **58**, 2209 (1987).

[9] G. L. Oppo, M. Brambilla, and L. A. Lugiato, Phys. Rev. A **49**, 2028 (1994).

[10] A. Yariv and P. Yeh, *Optical Waves in Crystals* (Wiley, New York, 1984).

[11] J. B. Geddes, J. Lega, J. V. Moloney, R. A. Indik, E. M. Wright, and W. J. Firth, Chaos Solitons Fractals **4**, 1261 (1994).

[12] M. Haelterman, S. Trillo, and S. Wabnitz, Opt. Commun. **93**, 343 (1993): A. J. Scroggie, W. J. Firth, G. S. McDonald, M. Tlidi, R. Lefever, and L. A. Lugiato, Chaos Solitons Fractals **4**, 1323 (1994).

[13] M. Tlidi and M. Haelterman (unpublished).

[14] R.-D. Li, P. Mandel, and T. Erneux, J. Opt. Soc. Am. B **8**, 1835 (1991); P. Mandel, *Theoretical Problems in Cavity Nonlinear Optics* (Cambridge University Press, Cambridge, 1997).

[15] M. Tlidi and P. Mandel, Chaos Solitons Fractals **4**, 1457 (1994).